HHS Public Access

Author manuscript

Magn Reson Med. Author manuscript; available in PMC 2021 September 01.

Published in final edited form as:

Magn Reson Med. 2020 September ; 84(3): 1661–1671. doi:10.1002/mrm.28211.

A within-coil optical prospective motion correction system for brain imaging at 7T

Phillip DiGiacomo[1], **Julian Maclaren**[2], **Murat Aksoy**[2], **Elizabeth Tong**[2], **Mackenzie Carlson**[1], **Bryan Lanzman**[2], **Syed Hashmi**[2], **Ronald Watkins**[2], **Jarrett Rosenberg**[2], **Brian Burns**[3], **Timothy W. Skloss**[4], **Dan Rettmann**[5], **Brian Rutt**[1,2], **Roland Bammer**[6], **Michael Zeineh**[2,&]

[1]Department of Bioengineering, Stanford University, Stanford, CA, United States

[2]Department of Radiology, Stanford University, Stanford, CA, United States

[3]Applied Sciences Lab West, GE Healthcare, Menlo Park, CA, United States

[4]MR Advanced Systems, GE Healthcare, Waukesha, WI, United States

[5]MR Applications and Workflow, GE Healthcare, Rochester, MN, United States

[6]Department of Radiology, University of Melbourne, Melbourne, Australia

Abstract

Purpose: Motion artifact limits the clinical translation of high-field MR. We present an optical prospective motion correction (PMC) system for 7T using a custom-built, within-coil camera to track an optical marker mounted on a subject.

Methods: The camera was constructed to fit between the transmit and receive coils with direct line-of-sight to a forehead-mounted marker, improving upon prior mouthpiece work at 7T. We validated the system by acquiring a 3D-IR-FSPGR on a phantom with deliberate motion applied. The same 3D-IR-FSPGR and a 2D-gradient echo (GRE) were then acquired on seven volunteers, with/without deliberate motion and with/without motion correction. Three neuroradiologists blindly assessed image quality. In one subject, an ultra-high-resolution 2D-GRE with 4 averages was acquired with motion correction. Four single-average acquisitions were then acquired serially, with the subject allowed to move between acquisitions. A fifth single-average 2D-GRE was acquired following subject removal and reentry.

Results: In both the phantom and human subjects, deliberate and involuntary motion were well-corrected. Despite marked levels of motion, high-quality images were produced without spurious artifacts. The quantitative ratings confirmed significant improvements in image quality in the absence and presence of deliberate motion, across both acquisitions ($p<0.001$). The system enabled ultra-high-resolution visualization of the hippocampus during a long scan, and robust alignment of serially-acquired scans with interspersed movement.

Conclusion: We demonstrate the use of a within-coil camera to perform PMC and ultra-high-resolution imaging at 7T. The setup does not require a mouthpiece, which could improve accessibility of motion correction during 7T exams.

[&]Corresponding Author: (t: (650)-722-2235 mzeineh@stanford.edu).

Keywords

prospective motion correction; optical motion correction; ultra-high field MRI; neuroimaging

Introduction:

Ultra-high-field (7T) MRI systems can produce images with higher signal-to-noise ratio (SNR) and spatial resolution than lower-field strength MR systems (1.5T, 3T). In recent years, ultra-high-field MRI has been used to elucidate novel insights into the pathology of neurological and neuropsychiatric diseases ex vivo.[1–4] These findings have led to a growing number of in vivo studies performed at 7T, where increased resolution of structural and functional scans has led to enhanced visualization of microstructures[5–6] and novel networks of brain connectivity,[7] enabling insights into the pathology of a range of neurological diseases.[8–13] However, achieving both high SNR and high resolution requires long scan times. Though work is currently being done to accelerate scans at 7T,[14] the requisite long scan times often result in image artifacts due to subject motion. These motion artifacts limit the clinical interpretability of images and the reliability of quantitative analyses, such as segmentations that estimate volume and thickness. For these reasons, it is critical to prevent or correct for motion artifact in 7T MR images, particularly those acquired at very high resolution, to identify and develop novel imaging-based biomarkers of disease.

Retrospective methods for motion correction are available,[15–17] but require longer post-processing time and may be insufficient, due to overlaps and gaps in k-space.[18] Prospective motion correction can overcome this limitation by using measured head position and orientation to update the imaging volume position and orientation within the bore in real-time. The necessary real-time head pose information can be obtained using several techniques, including active markers,[19] field probes,[20–21] sequence-navigator-based methods,[22] or optical tracking using a camera system.[23–24] In the latter case, since the camera is independent of the MRI scanner, application to most clinical sequences is possible with real-time adjustment of k-space trajectories. Prior work has shown that PMC systems can enable higher resolution structural imaging in volunteers than would otherwise be achievable[25–26] and can provide improved quantitative susceptibility maps.[27]

Despite these promising results, one obstacle that remains in translating optical PMC to high-field MRI and routine clinical use is maintaining sufficiently clear line-of-sight from the camera to a head-mounted optical marker. Early proof-of-concept studies used multiple cameras external to the bore of the MRI scanner,[28–29] making line-of-sight for long or narrow-bore magnets, enclosed head coils, or large subjects a challenge, limiting clinical utility. The development of MR-compatible cameras has made it possible to use cameras within the B_0 field of the scanner, for example, attached to the inner surface of the bore or to a rig placed around the receive-only head coil.[24] Our prior work at 3T used a single camera mounted directly on the receive-only head coil, such that an unimpeded view of an optical marker to the subject's head can be achieved between the rungs of the coil.[30–31] However, since most commercial 7T systems do not use a body RF transmit coil due to heating limitations, available head coils at 7T are typically enclosed within an RF transmit shell,

making an unimpeded and reliable line-of-sight to a head-mounted marker a challenge, leading to the use of mouthpieces to extend marker visibility beyond the head coil at 7T.[25–27] Addressing this challenge is critical to translating the ultra-high-resolution imaging that has been achieved using these systems to broader research and clinical use.

The present work fully addresses this challenge through the design of a slim, custom-built camera that fits between shells of Nova Medical 32 receive (Rx) head coils (either 2ch Tx or 8ch transmit (Tx) versions) used in 7T GE scanners. The direct line-of-sight enables visualization of an optical marker on the subject's forehead. An adhesive backing provides a rigid coupling between the subject's forehead and the marker, with improved patient tolerance compared to a mouthpiece. Here, we acquire data on seven compliant subjects to demonstrate that the resulting PMC system has the ability to detect and correct for both rigid-head and physiologic motion across various sequences (3D-IR-FSPGR and 2D-GRE). Moreover, we demonstrate that this system provides the ability to obtain high-fidelity acquisitions of ultra-high-resolution scans that are otherwise too long for clinical use. This system can also be used to robustly align serially acquired scans with patients moving and even leaving the scanner as long as the marker remains attached in the same position. By allowing the acquisition of ultra-high-resolution scans free from motion artifact, the use of this system at 7T in research and clinical settings is expected to facilitate the discovery of novel neuroimaging biomarkers. Parts of this study have been previously published in abstract form.[32]

Methods:

Manufacturing and hardware:

A single non-commercial, MR-compatible camera was designed and built to be mounted between the Tx and Rx shells of Nova Medical 32ch Rx head coils (either 2ch or 8ch Tx versions) used in 7T GE scanners (Figure 1A). The camera prototype has a resolution of 640×480 and maximum frame rate of 100 Hz. The internal circuitry has been modified from our previous work at 3T MR-PET[26] to fit in the shielded, 45mm × 144 mm assembly. This assembly is attached to a rig which mounts to the head coil (see SI Figure S1). The camera is currently powered using two small, non-magnetic lithium polymer batteries, connected in series and covered in copper tape, to form a shielded 7.4 V battery pack. The voltage is dropped to 5V inside the camera using a linear regulator. The battery pack is connected to the camera housing using a non-magnetic SMB connector, which effectively connects the shield of the camera housing to the shield of the battery. This setup gives a usable runtime of about an hour before the battery pack must be recharged, which takes roughly 30 minutes. The positioning of the camera within the coil enables direct line-of-sight to a checkerboard-marker placed with adhesive on the left side of a subject's forehead with the subject in the typical recumbent position within the head coil (Figure 1B–C). This marker has a defined geometry and each square on the checkerboard contains a unique barcode which allows custom software to easily identify the marker within the camera's field-of-view.[33] Video of the marker and plots of motion are displayed in real-time: we visually assessed these and confirmed that scanning does not affect video or tracking quality. Motion correction is applied once at the beginning of each TR to avoid any delays in the sequence. The custom

software determines the position of the marker and updates the scanner gradients accordingly.

Calibration:

The location of the camera within the MRI bore was calibrated as in our prior work at 3T,[24] but adapted for 7T. A calibration apparatus, which incorporated wireless active markers, was built, and tuned to 298 MHz. Motion was applied to the calibration apparatus, enabling a rapid (<30 second) cross-calibration, whereby the coordinate transformation between the camera and scanner coordinates was calculated. The table position in the Z-direction is stored at the time of the calibration, so any change in table position (which is constantly updated by the table position encoder) relative to this initial position can be used to update the coordinate transformation. This allows the head coil to be moved synchronously with the table, without losing knowledge of the camera position in the scanner reference frame.[30] This detailed calibration is needed only once. During scanning, the cross-calibration, the table position at the time of cross-calibration, and the current table position are used to continuously update the coordinate transformation.

At the beginning of each subject scan, a modified scout localizer is acquired once following landmarking to initialize the PMC system and set an initial reference point for head position. This localizer only needs to be reacquired if the marker were placed in a different position on the subject's forehead, or if the table were pulled completely out such that repeat landmarking was required.

Phantom Validation:

Validation to test the effect of the hardware installation on scanner stability was performed on an agar gel phantom. First, to confirm that the hardware does not cause field distortions or impact temporal stability, high-resolution echo planar imaging (EPI) (1mm × 1mm × 3mm resolution, 9 slices, TR=2000ms, TE=30ms, flip angle = 90, 1000 timepoints) was acquired without (twice) and with (once) the hardware installed. Then, to test whether the hardware absorbs RF energy, we measured the transmit gain (TG) and specific absorption rate (SAR) accumulation during a high flip angle 2D gradient echo (GRE) sequence (256×128, FOV 17, slice thickness 2.0, spacing 6.0, TE 20, TR 550, FA 120, bandwidth 19.23V, 1m14s scan time) acquired without and with the camera hardware installed. Subsequent validation of the PMC system's motion tracking was conducted using a phantom with complex internal features (a papaya fruit). Deliberate continuous, rotational motion was applied using a wooden rod attached rigidly to the papaya during a T1-weighted 3D-IR-FSPGR sequence (see SI Table S1 for full sequence parameters). The sequence was acquired twice, once without and once with motion correction.

In Vivo Testing:

Subjects: Seven cooperative healthy subjects (5 female, median age of 28 years (range 25–45)) were recruited to participate in the study, with the approval of Stanford's Institutional Review Board (IRB) and in accordance with the Health Insurance Portability and Accountability Act (HIPAA) after obtaining informed consent.

Imaging Protocols (SI Table 1):

a. Test 1: To test the system in vivo, the same 3D-IR-FSPGR, as well as a 2D-T2-weighted oblique GRE sequence, were each acquired four times on each subject during the same scan session: no motion with and without correction, and with motion (asked to make discrete rotations ~15 degrees to the left or right every 30 seconds) with and without correction. This complete protocol was run on all 7 subjects.

b. Test 2: To test the system's ability to generate high-quality ultra-high-resolution images from otherwise untenably long acquisitions (>20 minutes), a 2D-GRE sequence with 4 averages was acquired on Subject 1 without motion and with motion correction.

c. Test 3: Since a continuous 20-minute scan is likely untenable in many clinical populations, an alternative ultra-high-resolution, 2D-GRE acquisition was obtained by averaging a series of 4 serially-acquired single average acquisitions without motion and with correction on Subject 1. The subject was allowed to relax, stretch and rotate their head between acquisitions.

d. Test 4: A fifth single average ultra-high-resolution, 2D-GRE acquisition was acquired on Subject 1 following the subject table being removed from the bore and the subject being asked to sit upright, followed by placing the subject back in the scanner. This was to assess the ability of optical prospective correction to correct for motion and changes in positioning in clinical settings when subjects may need to leave the bore (e.g. to use the bathroom or take a break during scanning, both of which commonly occur clinically).

Recorded tracking data were used to quantify and calculate summary statistics of 3D translational and rotational motion for each acquisition.

Quantitative Analysis:

Three blinded, experienced neuroradiologists (authors BL, SH, and MZ with 4, 3, and 11 years of post-residency neuroradiology experience, respectively) separately evaluated the 3D-IR-FSPGR and 2D-GRE images from Test 1 for motion-related artifacts (e.g. ringing, blurring, ghosting, and striping), attributing an assessment of scan quality on a 5-point scale (with a 1 representing excellent image quality and a 5 representing completely corrupted by artifact) to each acquisition, based in part on previous criteria.[34] The neuroradiologists then assessed the 3D-IR-FSPGR acquisitions for visualization of the gray-white matter junction, and the 2D-GRE acquisitions for visualization of deep gray nuclei (subthalamic and red nuclei and substantia nigra) and the hippocampus, separately, on 5-point scales based in part on previous criteria.[35] These features were selected because they are of different size and contrast, and are clinically relevant. Data from two subjects were used as test images to train the raters and reach agreement on each scale. Data from the remaining five subjects were then used for analysis. The order in which the datasets and sequences were presented was randomized across readers. Overall agreement among readers was high (Krippendorf's alpha coefficient = 0.89, 95% CI: 0.87–0.92). The effects of deliberate motion, motion correction, their interaction, and acquisition type were tested on each scale with generalized linear

regression models with log link, adjusted for clustering within subject and reader. All statistical analyses were done with Stata Release 15.1 (StataCorp LP, College Station, TX). A p-value less than 0.05 was considered significant.

Results:

Phantom Validation:

Validation tests performed on an agar gel phantom without and with the hardware installed showed no change in echo-planar distortion or signal variance over time (SI Figure S2A–B). Likewise, the magnitude difference maps computed between the with and without camera acquisitions (SI Figure S2C) show similar magnitude to those from duplicate acquisitions without the camera (SI Figure S2D). In the 2D-GRE experiment, the addition of the camera hardware caused an increase in TG from 163 to 173 (1.0 dB), which corresponds to a 12.2% increase in transmit voltage. We also measured a 26% increase in apparent SAR (2.3 W/kg without camera, 2.9 W/kg with camera). The papaya phantom validation study reveals a reduction in motion artifact with PMC (SI Figure S3). The uncorrected acquisition (SI Figure S3A) is heavily corrupted by artifact, limiting contrast of the fine detail of the interior, seed-containing portion of the papaya. The corrected acquisition (SI Figure S3B) shows more clearly delineated boundaries despite similar levels of motion.

In Vivo Testing:

a. Test 1: The 3D-IR-FSPGR (Figures 2A, 2C) and 2D-GRE (Figures 2E, 2G) images acquired without deliberate rotational motion display modest levels of translational (<2mm) and rotational (<2 degrees) motion (SI Tables S2–3), demonstrating that motion is present and can potentially corrupt images even in short scans (<5 minutes) acquired on compliant healthy subjects (see SI Figure S4 for additional example dataset). In the acquisitions with deliberate motion, the range and standard deviation of motion appear comparable between uncorrected and corrected sequences (SI Tables S2–3). These marked levels of both translational (~ 2mm) and rotational (>5 degrees) motion resulted in poor and almost unusable image quality without correction (Figures 2B, 2F). Resultant artifact was markedly reduced with motion-correction, enabling visualization of both gray-white differentiation (Figure 2D) and deep-gray and brainstem nuclei (Fig.2H), though some residual artifact remains (see SI Figure S4 for an additional example dataset).

The quantitative rater analysis confirmed these observations (SI Table S4). Statistically significant improvements in image quality were seen with motion correction in both acquisitions ($p<0.001$), minimally stronger on the 3D-IR-FSPGR acquisitions ($p=0.045$). The effect of motion correction was stronger in acquisitions with deliberate motion ($p=0.021$). Likewise, for gray-white junction visualization on the 3D-IR-FSPGR acquisitions, ratings were overall worse with motion ($p<0.001$), and better with motion correction ($p=0.043$), with the effect of motion correction stronger in the presence of motion ($p<0.001$). Similarly, for both deep gray nuclei and hippocampal visualization on the 2D-GRE

acquisitions, ratings were overall worse with motion ($p<0.001$), and better with motion correction ($p<0.001$), with the effect of motion correction stronger in the presence of motion ($p=0.011$). On all subjects, the PMC-corrected image quality was the same or better on visual rating for 3D-IRFSPGR across the majority of raters for matched motion/no-motion pairs. The same was true for GRE except for one subject with intentional motion, in which the uncorrected GREs was rated a 4 and the corrected GREs a 5 on all metrics (both ratings are unusable for clinical diagnosis). Thus, no acquisitions showed a clinically meaningful worsening with the addition of motion correction.

b. Test 2: The 20-minute ultra-high-resolution 2D-GRE acquisition showed more than double the range and standard deviation of motion compared to the shorter 4-minute acquisitions (Figure 3, SI Table S5) on the same subject. Both rigid-head and physiological respiratory motion were detected (Figure 3). Motion-corrected images demonstrated exquisite quality despite the long scan time, providing high-resolution visualization of the hippocampus and deep gray nuclei.

c. Test 3: For the serially-acquired single average scans, real-time recording of subject position during and between acquisitions provided robust registration across acquisitions without any additional post-processing (Figure 4, SI Table S6). The averaged images are of comparable quality to the longer, 4-average scan, demonstrating the ability of the PMC system to facilitate ultra-high-resolution scans over shorter, clinically-practical time scales (Figure 4).

d. Test 4: At the start of the fifth single average acquisition, following the subject being removed from the bore and stepping off of the table, the subject's initial position was markedly different from the original calibrated position (~2 mm and ~4 degrees), but image quality remained high with images well-registered across acquisitions (Figure 5, SI Table 6), demonstrating that the system remains effective even when the subject leaves the bore during an exam.

Discussion:

In this study, we successfully implemented an optical PMC system for brain imaging at 7T using a custom-built, within-coil camera and head-mounted optical marker for tracking. Using this system, detection of both deliberate and involuntary (rigid-head, respiratory, and cardiac) motion was demonstrated on human subjects, and motion correction produced high-quality images, without introducing spurious artifacts. We demonstrated the system's ability to make possible otherwise untenably long scans, enabling ultra-high-resolution imaging. Finally, we demonstrated that our approach enables robust alignment of serially acquired scans, providing subjects the opportunity to leave the bore between scans, while still allowing acquisition of high-fidelity images. The key advantage of PMC in this setting is that we can achieve high SNR using averaging of scans with clinically tractable scan durations without the need for image registration which can be difficult for slabs with limited coverage and can introduce blurring. Our rater analysis demonstrates that PMC with this system provides significantly improved overall image quality (i.e. reduced motion artifact) and allows for better visualization of clinically-important structures: the gray-white

junction (focal cortical dysplasias[36]), the deep gray nuclei (movement disorders[37]), and the hippocampus (neurodegenerative diseases,[38] epilepsy,[39] and mild traumatic brain injury[40]). The effect of motion correction is seen in healthy, compliant subjects with minimal motion, but a larger improvement is seen in the context of larger magnitude motion. This suggests the system will provide significant benefit when scanning clinical populations who are prone to move during scans, allowing for more nuanced diagnosis and staging of disease and the development of novel biomarkers.

Our approach builds on the work of the Magdeburg group, which pioneered the use of optical prospective motion correction at 7T using a mouthpiece.[25–29] Our within-coil camera provides clear line-of-sight to the optical marker on the subject's forehead, eliminating the need for the mouthpiece. Mouthpieces are rigidly bound to the upper teeth but remain difficult to implement clinically because they are time-consuming to make, less comfortable for patients, make it difficult for patients to communicate with technicians, and are influenced by chewing and tongue motion. A limitation of attaching the marker to the forehead is that the skin can move relative to the skull, but the use of medical adhesive (Opsite Flexifix) placed tightly on the forehead while the skin above the eyebrow is stretched before placement of the marker appears effective at reducing this. Likewise, hair can obscure the view of the marker and needs to be pulled back. Prior to scanning, the only additional step required for technologists is placing the marker on the subject's forehead. The simplicity and comfort of this optical PMC system makes translation to clinical use practical. While under certain scanning conditions, the required power is increased with the camera in place, this is at most a ~25% increase, and it is likely that some of this energy is deposited in the camera, not the patient. We do not believe that this increase will be prohibitive for clinically-relevant scanning protocols. Our future work will include better characterization and reduction of this increase in required power.

The current system is limited by the latency between the scanner and PMC. Previous studies by our group on earlier camera prototypes and the same marker at 3T showed a latency time of ~24 ms,[41] so very fast motion such as coughing may not be fully corrected and may cause residual motion artifacts. The theoretical limit for latency is based on the frame rate of the camera (in our system, 10 ms given the 100Hz frame rate) plus the time needed to determine marker position (which could be reduced with faster image processing) and update the scanner gradients. Additionally, optical PMC systems correct for real-time changes in the position and orientation of the head within the scanner, but not for residual field perturbations, which could still cause artifacts. Another limitation of this experimental prototype is that the power supply is an external battery with finite charge, limiting the length of protocols that can be performed in a single sitting currently. Finally, the current prototype of this system has the camera mounted to the same location where mirrors are mounted for task-based functional imaging, meaning this system cannot be used during protocols with visual stimuli. Alternative camera mounting designs that would provide a line-of-sight to a bite bar marker could also be envisioned.

The presented results should be interpreted within the limitations of this study. To compare the effect of motion correction on image quality, scans were repeated sequentially with and without motion correction. While subjects' deliberate motion cannot be entirely identical

between repetitions of sequences, the quantitative motion tracking data measured here shows similar magnitudes and frequency of motion between scans. Moreover, the motion conditions tested in this study were of compliant, healthy subjects either holding as still as possible or making exaggerated motions. It is possible that the motion produced by clinical subjects may differ. This should be considered when translating to clinical populations. Moreover, we have tested our system on only two specific sequences in this paper. Ongoing work aims to extend these PMC methods to additional sequences, including multi-echo sequences, echo-planar imaging, and high-resolution T1-weighted sequences, to confirm that the conclusions of this study can be applied to additional sequences relevant for 7T brain exams. Future work should also include quantitative assessment of image quality, in addition to the rater analysis already performed.

This work demonstrates that this optical PMC system may overcome motion artifact in brain imaging at 7T, one of the biggest challenges precluding utilization of ultra-high-field MR in both research and clinical settings. This practical, user-friendly design allows longer scan-times and finer image resolution, providing potential to facilitate the discovery of novel biomarkers of aging and disease.

Supplementary Material

Refer to Web version on PubMed Central for supplementary material.

Acknowledgements:

The authors of this manuscript are listed as inventors on numerous patents and patent applications relating to motion correction in MRI. Drs. Aksoy, Bammer, and Maclaren consult for HobbitView Inc., a company that aims to commercialize motion correction methods.

The authors would like to acknowledge research support by GE Healthcare, NIH P41 EB015891, NIH S10 RR026351-01A1, NIH R01 AG061120-01, and the ASNR Boerger Alzheimer's Fund. The authors would also like to thank Nicole Mouchawar for her assistance with manuscript preparation.

References:

1. De Reuck J, Deramecourt V, Auger F, Durieux N, Cordonnier C, Devos D, Defebvre L, Moreau C, Caparros-Lefebvre D, Bordet R, Maurage CA, Pasquier F, Leys D. Post-mortem 7.0-tesla magnetic resonance study of cortical microinfarcts in neurodegenerative diseases and vascular dementia with neuropathological correlates. J Neurol Sci. 2014; 346, 85–89. [PubMed: 25129206]
2. Yao B, Hametner S, van Gelderen P, Merkle H, Chen C, Lassmann H, Duyn JH, Bagnato F. 7 Tesla magnetic resonance imaging to detect cortical pathology in multiple sclerosis. PLoS One. 2014;9, e108863. [PubMed: 25303286]
3. Zucca I, Milesi G, Medici V, Tassi L, Didato G, Cardinale F, Tringali G, Colombo N, Bramerio M, D'Incerti L, Freri E, Morbin M, Fugnanesi V, Figini M, Spreafico R, Garbelli R. Type II focal cortical dysplasia: Ex vivo 7T magnetic resonance imaging abnormalities and histopathological comparisons. Ann Neurol. 2016;79, 42–58. [PubMed: 26448158]
4. Kenkhuis B, Jonkman LE, BulK M, Buijs M, Boon BD, Bouwman FH, Geurts JJ, van de Berg WD, van der Weerd L. 7T MRI allows detection of disturbed cortical lamination of the medial temporal lobe in patients with Alzheimer's disease. NeuroImage: Clinical. 2019; 101665.
5. Deistung A, Schäfer A, Schweser F, Biedermann U, Turner R, Reichenbach JR. Toward in vivo histology: a comparison of quantitative susceptibility mapping (QSM) with magnitude-, phase-, and R2*-imaging at ultra-high magnetic field strength. NeuroImage. 2013; 65, 299–314. [PubMed: 23036448]

6. Bianciardi M, Strong C, Toschi N, Edlow BL, Fischl B, Brown EN, Rosen BR, Wald LL. A probabilistic template of human mesopontine tegmental nuclei from in vivo 7 T MRI. NeuroImage. 2018; 170, 222–230. [PubMed: 28476663]
7. Muckli L, De Martino F, Vizioli L, Petro LS, Smith FW, Ugurbil K, Goebel R, Yacoub E. Contextual feedback to superficial layers of V1. Current Biology. 2015; 25(20), 2690–2695. [PubMed: 26441356]
8. de Graaf WL, Zwanenburg JJ, Visser F, Wattjes MP, Pouwels PJ, Geurts JJ, Polman CH, Barkhof F, Luijten PR, Castelijns JA. Lesion detection at seven Tesla in multiple sclerosis using magnetisation prepared 3D-FLAIR and 3D-DIR. Eur Radiol. 2012; 22, 221–231. [PubMed: 21874361]
9. van Veluw SJ, Zwanenburg JJM, Engelen-Lee J, Spliet WGM, Hendrikse J, Luijten PR, Biessels GJ. In vivo detection of cerebral cortical microinfarcts with high-resolution 7T MRI. Journal of Cerebral Blood Flow and Metabolism. 2013;33, 322–329. [PubMed: 23250109]
10. Harrison DM, Roy S, Oh J, Izbudak I, Pham D, Courtney S, Caffo B, Jones CK, van Zijl P, Calabresi PA. Association of Cortical Lesion Burden on 7-T Magnetic Resonance Imaging With Cognition and Disability in Multiple Sclerosis. JAMA Neurol. 2015;72, 1004–1012. [PubMed: 26192316]
11. De Ciantis A, Barba C, Tassi L, Cosottini M, Tosetti M, Costagli M, Bramerio M, Bartolini E, Biagi L, Cossu M, Pelliccia V, Symms MR, Guerrini R. 7T MRI in focal epilepsy with unrevealing conventional field strength imaging. Epilepsia. 2016;57, 445–454. [PubMed: 26778405]
12. Obusez EC, Lowe M, Oh SH, Wang I, Bullen J, Ruggieri P, Hill, Lockwood D, Emch T, Moon D, Loy G, Lee J, Kiczek M, Massand M, Statsevych V, Stultz T, Jones SE. 7T MR of intracranial pathology: Preliminary observations and comparisons to 3T and 1.5 T. Neuroimage. 2019; 168, 459–476.
13. Shah P, Bassett DS, Wisse LE, Detre JA, Stein JM, Yushkevich PA, Shinohoara RT, Elliot MA, Das SR, Davis KA. Structural and functional asymmetry of medial temporal subregions in unilateral temporal lobe epilepsy: A 7T MRI study. Human brain mapping. 2019.
14. Uğurbil K, Auerbach E, Moeller S, Grant A, Wu X, Van de Moortele PF, Olman C, Delaware L, Schillak S, Radder J, Lagore R, Adriany G. Brain imaging with improved acceleration and SNR at 7 Tesla obtained with 64-channel receive array. Magnetic Resonance in Medicine. 2019.
15. Gallichan D, Marques JP, Gruetter R. Retrospective correction of involuntary microscopic head movement using highly accelerated fat image navigators (3D FatNavs) at 7T. Magnetic Resonance in Medicine. 2016; 75: 1030–1039. [PubMed: 25872755]
16. Engström M, Mårtensson M, Avventi E, Norbeck O, Skare S. Collapsed fat navigators for brain 3D rigid body motion. Magnetic Resonance Imaging. 2015; 33(8), 984–991. [PubMed: 26117701]
17. Gallichan D, Marques JP. (2017). Optimizing the acceleration and resolution of three-dimensional fat image navigators for high-resolution motion correction at 7T. Magnetic Resonance in Medicine. 2017; 77(2), 547–558. [PubMed: 26877158]
18. Federau C, Gallichan D. Motion-Correction Enabled Ultra-High Resolution In-Vivo 7T MRI of the Brain. PLoS ONE. 2016; 11(5): e0154974. [PubMed: 27159492]
19. Ooi MB, Krueger S, Thomas WJ, Swaminathan SV, Brown TR. Prospective realtime correction for arbitrary head motion using active markers. Magnetic Resonance in Medicine. 2009;62(4):943–54. [PubMed: 19488989]
20. Haeberlin M, Kasper L, Barmet C, Brunner DO, Dietrich BE, Gross S, et al. Realtime motion correction using gradient tones and head-mounted NMR field probes. Magnetic Resonance in Medicine. 2014; 74(3), 647–660. [PubMed: 25219482]
21. Vannesjo SJ, Wilm BJ, Duerst Y, Gross S, Brunner DO, Dietrich BE, Schmid T, Barmet C, Pruessmann KP. Retrospective correction of physiological field fluctuations in high-field brain MRI using concurrent field monitoring. Magnetic Resonance in Medicine. 2015;73(5), 1833–1843. [PubMed: 24903278]
22. White N, Roddey C, Shankaranarayanan A, Han E, Rettmann D, Santos J, Kuperman J, Dale A. PROMO: real-time prospective motion correction in MRI using image-based tracking. Magnetic Resonance in Medicine. 2010:63(1), 91–105. [PubMed: 20027635]

23. Schulz J, Siegert T, Reimer E, Labadie C, Maclaren J, Herbst M, Zaitsev M, Turner R. An embedded optical tracking system for motion-corrected magnetic resonance imaging at 7T. Magnetic Resonance Materials in Physics, Biology and Medicine. 2012; 25(6), 443–453.
24. Maclaren J, Armstrong BSR, Barrows RT, et al. Measurement and correction of microscopic head motion during magnetic resonance imaging of the brain. PLoS One 2012;7: e48088. [PubMed: 23144848]
25. Stucht D, Danishad KA, Schulze P, Godenschweger F, Zaitsev M, Speck O. Highest Resolution In Vivo Human Brain MRI Using Prospective Motion Correction. PLoS One. 2015; 10: e0133921. [PubMed: 26226146]
26. Mattern H, Sciarra A, Godenschweger F, Stucht D, Lüsebrink F, Rose G, Speck O. Prospective motion correction enables highest resolution time-of-flight angiography at 7T. Magnetic Resonance in Medicine. 2018; 80: 248–258. [PubMed: 29230871]
27. Mattern H, Sciarra A, Lüsebrink F, Acosta-Cabronero J, Speck O. Prospective motion correction improves high-resolution quantitative susceptibility mapping at 7T. Magnetic Resonance in Medicine. 2018.
28. Zaitsev M, Dold C, Sakas G, Hennig J, Speck O. Magnetic resonance imaging of freely moving objects: prospective real-time motion correction using an external optical motion tracking system. Neuroimage 2006;31:1038–1050. [PubMed: 16600642]
29. Speck O, Hennig J, Zaitsev M. Prospective real-time slice-by-slice motion correction for fMRI in freely moving subjects. MAGMA. 2006; 19:55–61. [PubMed: 16779560]
30. Maclaren J, Aksoy M, Ooi MB, Zahneisen B, & Bammer R Prospective motion correction using coil-mounted cameras: Cross-calibration considerations. Magnetic Resonance in Medicine. 2018;79(4), 1911–1921. [PubMed: 28722314]
31. Spangler-Bickell MG, Khalighi MM, Hoo C, DiGiacomo PS, Maclaren J, Aksoy M, Rettmann D, Bammer R, Zaharchuk G, Zeineh M, Jansen F. Rigid Motion Correction for Brain PET/MR Imaging using Optical Tracking. IEEE Transactions on Radiation and Plasma Medical Sciences. 2018.
32. DiGiacomo PS, Tong E, Maclaren J, Aksoy M, Bammer R, Rutt B, Zeineh M. A novel, coil-integrated camera for prospective optical motion correction of brain imaging at 7T. International Society of Magnetic Resonance in Medicine, 2019, Montreal, Canada.
33. Forman C, Aksoy M, Hornegger J, Bammer R. Self-Encoded Marker for Optical Prospective Head Motion Correction in MRI. Medical Image Analysis. 2011; 15(5):708–19. [PubMed: 21708477]
34. Tanenbaum LN, Tsiouris AJ, Johnson AN, Naidich TP, DeLano MC, Melhem ER, Quarterman P, Parameswaran SX, Shankaranarayanan A, Goyen M, Field AS. Synthetic MRI for clinical neuroimaging: results of the Magnetic Resonance Image Compilation (MAGiC) prospective, multicenter, multireader trial. American Journal of Neuroradiology. 2017; 38(6), 1103–1110. [PubMed: 28450439]
35. Zeineh M, Parekh M, Zaharchuk G, Su J, Rosenberg J, Fischbein N, Rutt B. Ultra-High Resolution Imaging of the Human Brain with Phase-Cycled Balanced Steady State Free Precession at 7.0 T. Investigative Radiology. 2014; 49(5), 278. [PubMed: 24473366]
36. Blackmon K, Kuzniekcy R, Barr WB, Snuderl M, Doyle W, Devinsky O, Thesen T. Cortical Gray-White Matter Blurring and Cognitive Morbidity in Focal Cortical Dysplasia. Cerebral Cortex. 2015; 25(9), 2854–2862. [PubMed: 24770710]
37. Telford R, Vattoth S. MR Anatomy of Deep Brain Nuclei with Special Reference to Specific Diseases and Deep Brain Stimulation Localization. Neuroradiology Journal. 2014; 27(1), 29–43. [PubMed: 24571832]
38. Den Heijer T, van der Lijn F, Koudstaal PJ, Hofman A, van Der Lugt A, Krestin GP, Niessen WJ, Breteler MM. A 10-year follow-up of hippocampal volume on magnetic resonance imaging in early dementia and cognitive decline. Brain. 2010; 133(4), 1163–1172. [PubMed: 20375138]
39. Santyr BG, Goubran M, Lau JC, Kwan BYM, Salehi F, Lee DH, Mirsattari SM, Burneo JG, Steven DA, Parrent AG, de Ribaupierre S, Hammond RR, Peters TM, Khan AR. Investigation of hippocampal substructures in focal temporal lobe epilepsy with and without hippocampal sclerosis at 7T. Journal of Magnetic Resonance Imaging. 2017; 45:1359–1370. [PubMed: 27564217]

40. Parivash S, Goubran M, Mills BD, Rezaii P, Thaler C, Wolman D, Bian W, Mitchell LA, Boldt B, Douglas D, Wilson EW, Choi J, Xie L, Yushkevich PA, DiGiacomo P, Wongsripuemtet J, Parekh M, Fiehler J, Do H, Lopez J, Rosenberg J, Camarillo D, Grant G, Wintermark M, Zeineh M. Longitudinal Changes in Hippocampal Subfield Volume Associated with Collegiate Football. 2019; (ja).

41. Maclaren J Ooi, Aksoy, Ehrl, Bammer. Calibration and quality assurance for optical prospective motion correction using active markers. International Society of Magnetic Resonance in Medicine, 2014, Milan, Italy.

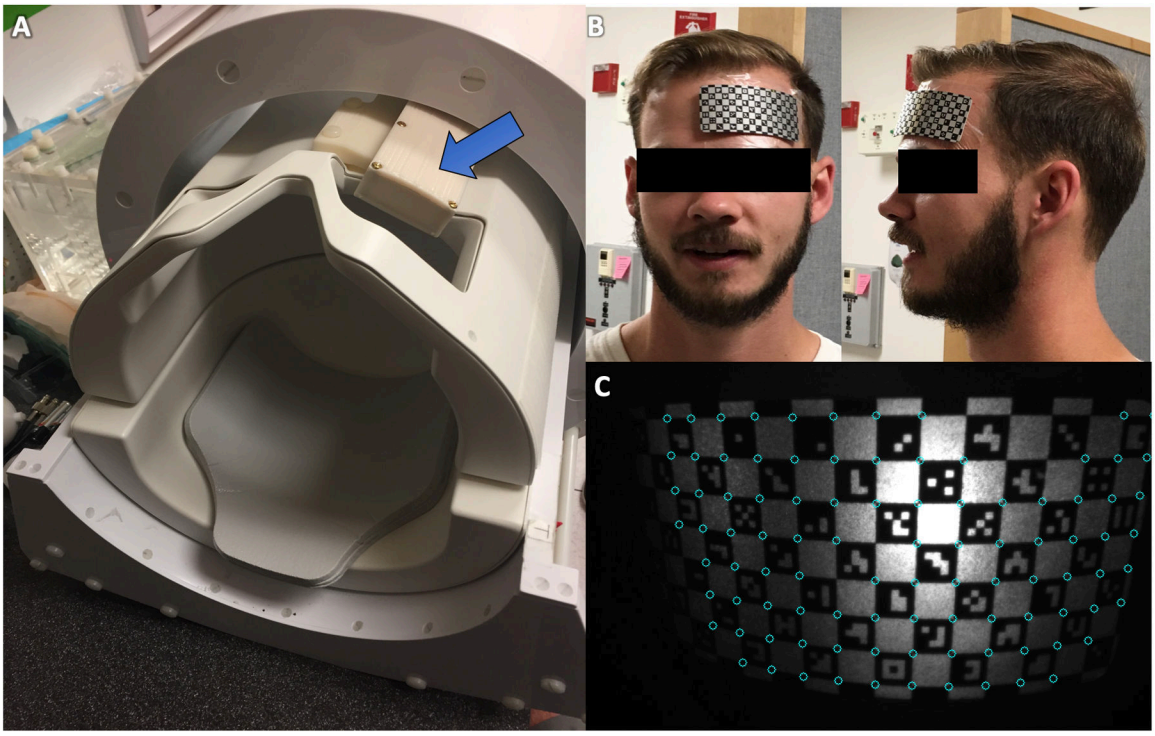

Figure 1:
The prospective motion correction (PMC) system in this study utilizes a MR-compatible camera (A) incorporated between the transmit and receive portions of the head coil to track a checkerboard optical marker (B) placed on the subject's forehead (C) for rigid tracking. Custom software identifies vertices between the barcodes to update the head position and modify gradients accordingly.

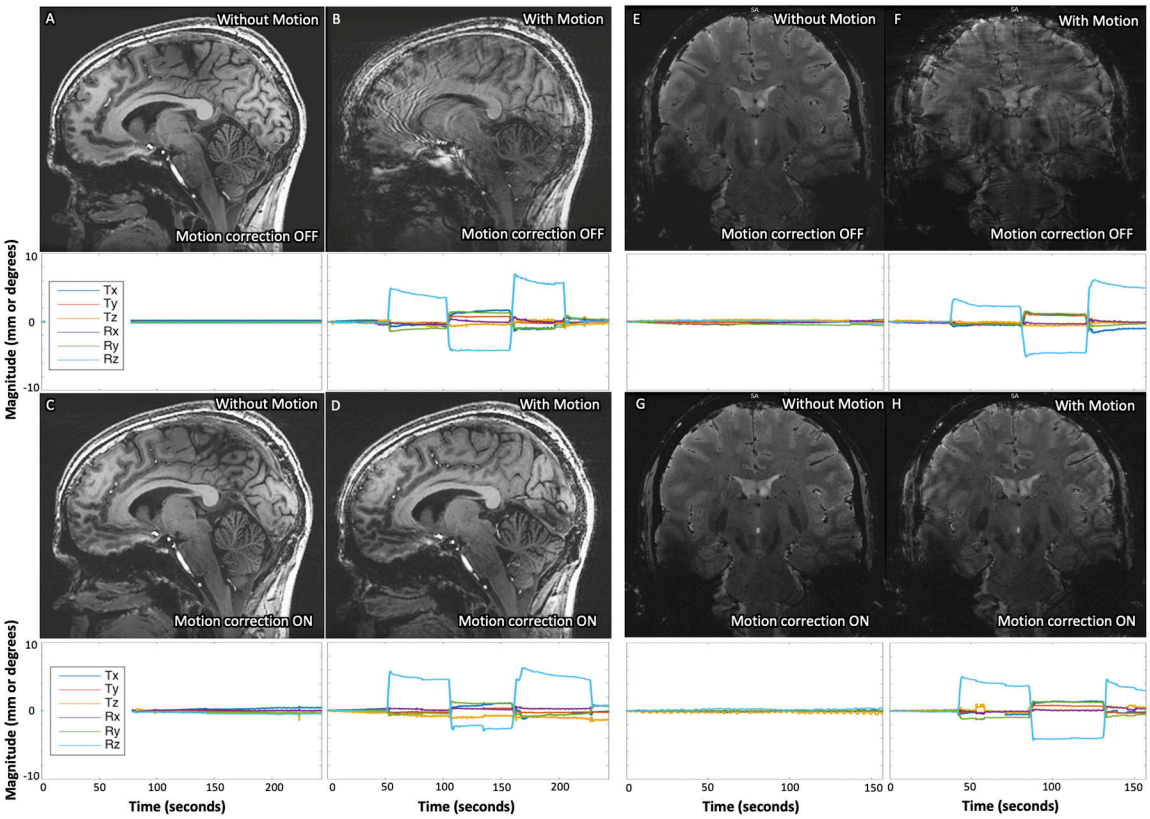

Figure 2:

Results of 3D IR-FSPGR (A-D) and 2D GRE (E-H) sequences acquired (A and E) without deliberate motion and without motion-correction, (B and F) with deliberate motion and without motion-correction, (C and G) without deliberate motion and with motion-correction, and (D and H) with deliberate motion and with motion-correction on Subject 1. Clear improvement of deliberate motion artifact can be seen in the corrected acquisitions (comparing B with D, and F with H). The plots below each image display the translational and rotational motion across time, with the vertical axis showing mm and degrees of displacement or rotation, respectively, and the horizontal showing time in seconds. Each direction of motion was normalized to the subject's initial position for that scan to visualize only net motion during the acquisition.

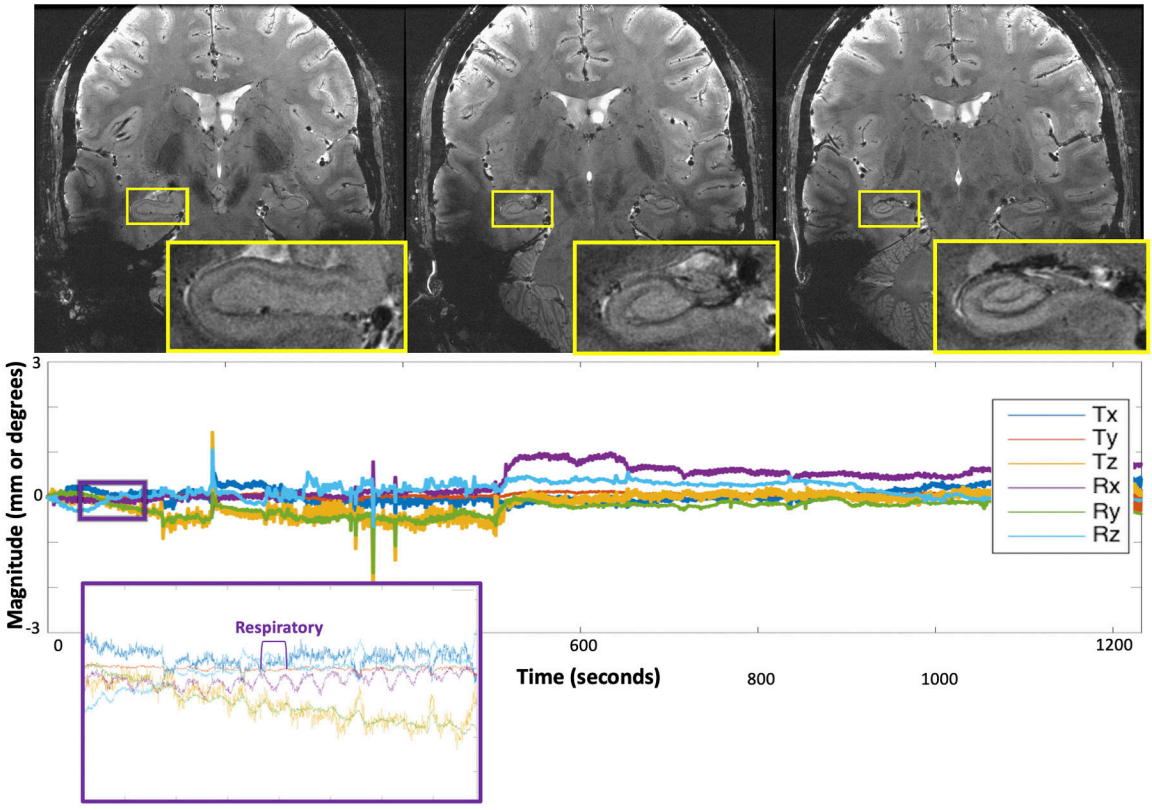

Figure 3:

Results of the 20-minute ultra-high-resolution 2D GRE sequence, demonstrating exquisite quality imaging of the hippocampus and remainder of the visualized brain. The plots below each image display the translational and rotational motion across time, with the vertical axis showing mm and degrees of displacement or rotation, respectively, and the horizontal showing time in seconds. Each direction of motion was normalized to the subject's initial position for this scan to visualize only net motion during the acquisition. The purple and orange insets show detection of physiologic respiratory motion, respectively, in addition to rigid-head motion.

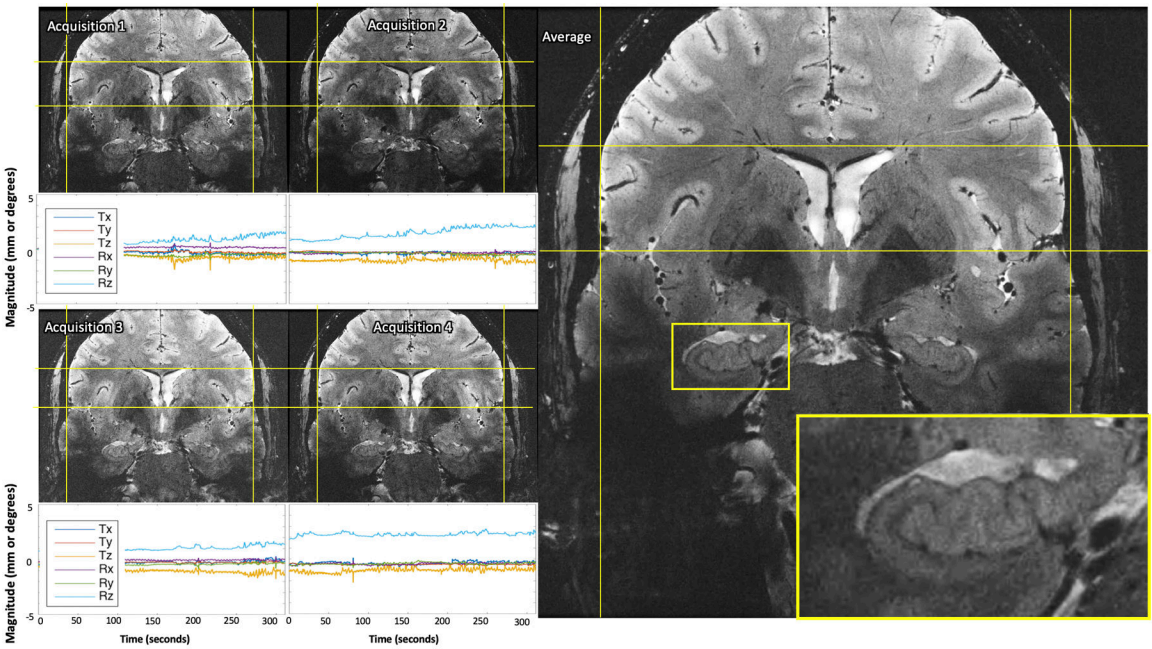

Figure 4:

Results of serially-acquired single average ultra-high-resolution images (A-D) remained well-aligned between acquisitions and comparable quality when averaged (E), despite motion during each scan. The plots below each image display the translational and rotational motion across time, with the vertical axis showing mm and degrees of displacement or rotation, respectively, and the horizontal showing time in seconds. Each direction of motion was normalized to the subject's initial position at the beginning of the first single average ultra-high-resolution acquisition to visualize net motion during all serial acquisitions.

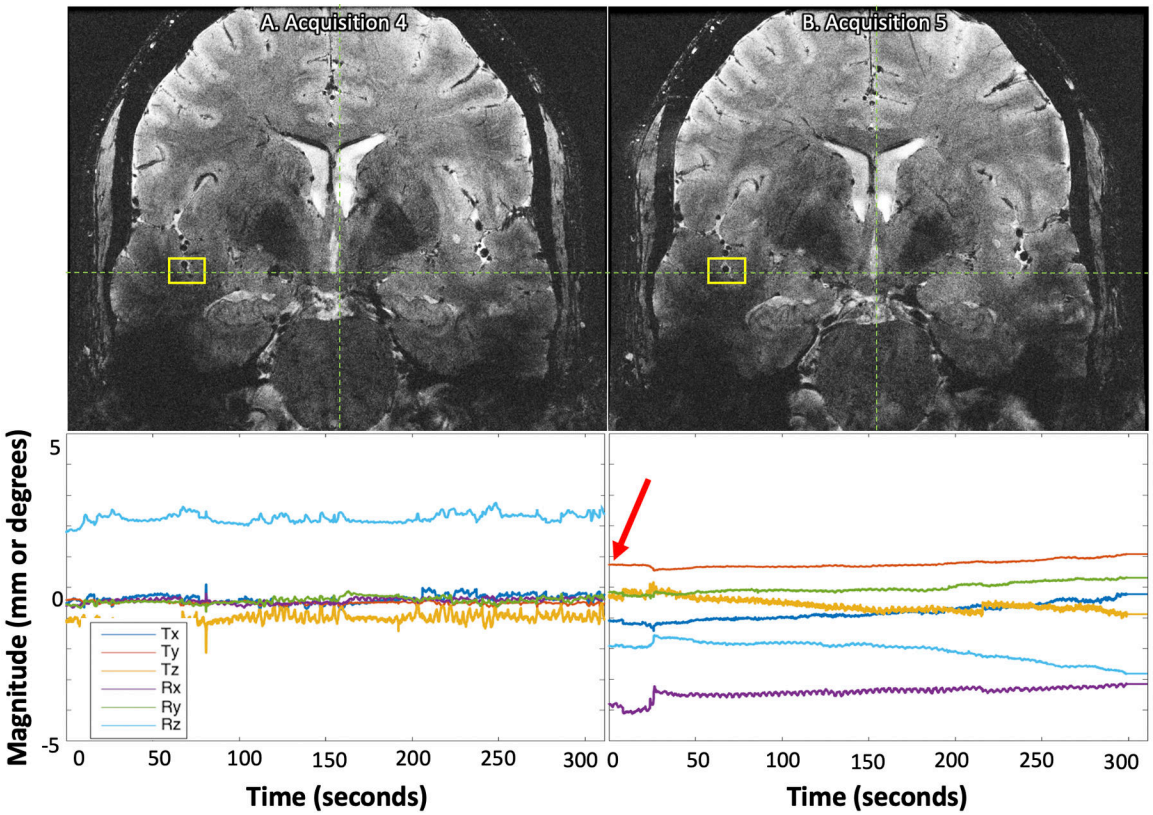

Figure 5:

Despite the subject being removed from the bore between the fourth (A) and fifth (B) single average ultra-high-resolution acquisitions and the subject's initial position for the fifth acquisition being noticeably different than the initial calibration point (B, red arrow), the images are well-aligned (yellow boxes). The plots below each image display the translational and rotational motion across time, with the vertical axis showing mm and degrees of displacement or rotation, respectively, and the horizontal showing time in seconds. Each direction of motion was normalized to the subject's initial position at the beginning of the first single average ultra-high-resolution acquisition to visualize net motion during all serial acquisitions.